Migration of cytotoxic lymphocytes in cell cycle permits local MHC I–dependent control of division at sites of viral infection

Silvia S. Kang,[1] Jasmin Herz,[1] Jiyun V. Kim,[2] Debasis Nayak,[1] Phillip Stewart-Hutchinson,[2] Michael L. Dustin,[2] and Dorian B. McGavern[1]

[1]National Institute of Neurological Disorders and Stroke, National Institutes of Health, Bethesda, MD 20892
[2]Molecular Pathogenesis Program, Helen L. and Martin S. Kimmel Center for Biology and Medicine, Skirball Institute of Biomolecular Medicine, New York University School of Medicine, New York, NY 10016

After virus infection, cytotoxic T lymphocytes (CTLs) divide rapidly to eradicate the pathogen and prevent the establishment of persistence. The magnitude of an antiviral CTL response is thought to be controlled by the initiation of a cell cycle program within lymphoid tissues. However, it is presently not known whether this division program proceeds during migration or is influenced locally at sites of viral infection. We demonstrate that antiviral CTLs remain in cell cycle while transiting to infected tissues. Up to one third of virus-specific CTLs within blood were found to be in cell cycle after infection with lymphocytic choriomeningitis virus or vesicular stomatitis virus. Using two-photon microscopy, we found that effector CTL divided rapidly upon arrest in the virus-infected central nervous system as well as in meningeal blood vessels. We also observed that MHC I–dependent interactions, but not costimulation, influenced the division program by advancing effector CTL through stages of the cell cycle. These results demonstrate that CTLs are poised to divide in transit and that their numbers can be influenced locally at the site of infection through interactions with cells displaying cognate antigen.

CORRESPONDENCE
Dorian B. McGavern:
mcgavernd@mail.nih.gov

Abbreviations used: Arm, Armstrong; CNS, central nervous system; i.c., intracerebrally; LCMV, lymphocytic choriomeningitis virus; VSV, vesicular stomatitis virus.

The magnitude of a virus-specific CTL response is dictated by clonal expansion (van Heijst et al., 2009), and the number of CTLs at peripheral sites of infection can tip the balance in favor of viral clearance or persistence. CTL numbers can also contribute to the severity of immunopathological reactions. Local CTL expansion increases the quantity of virus-specific T cells needed to offset exponential tissue viral replication; however, T cell division is thought to be a relatively slow process. Naive CD8^{+} T cells experience a 27-h lag phase followed by early division times of ~19 h (Veiga-Fernandes et al., 2000). Even at the peak of the proliferative response, CTL division is still estimated to occur every 6–8 h in the lymphoid organs (Murali-Krishna et al., 1998) where APC stimulation would theoretically be optimal. With such long division times, it is unclear how local peripheral responses out-compete viral dissemination. Because initial priming of CD8^{+} T cells with antigen presented on MHC I and cytokines imparts a differentiation program that dictates subsequent division and effector responses, it is

thought that additional division can occur in the absence of further antigen–MHC I interactions (Iezzi et al., 1998; van Stipdonk et al., 2001, 2003; Gett et al., 2003; Mescher et al., 2006; Agarwal et al., 2009). Therefore, emigration of T cells from lymphoid compartments while still in cell cycle may represent a critical mechanism that allows immediate turnover and additional instruction within peripheral sites of infection.

Another crucial question is whether the CTL cell division program can be altered by serial interactions received in one or multiple tissues. In lymphoid tissues, T cell priming is defined by a series of dynamic interactions, some of which are transient in nature. For example, CD4^{+} T cells initially develop transient interactions with the cognate peptide–MHC II–bearing DCs that are followed by the formation of long-lived T cell clusters where sustained contact is maintained for >1 h. By 16–24 h after encounter, T cell
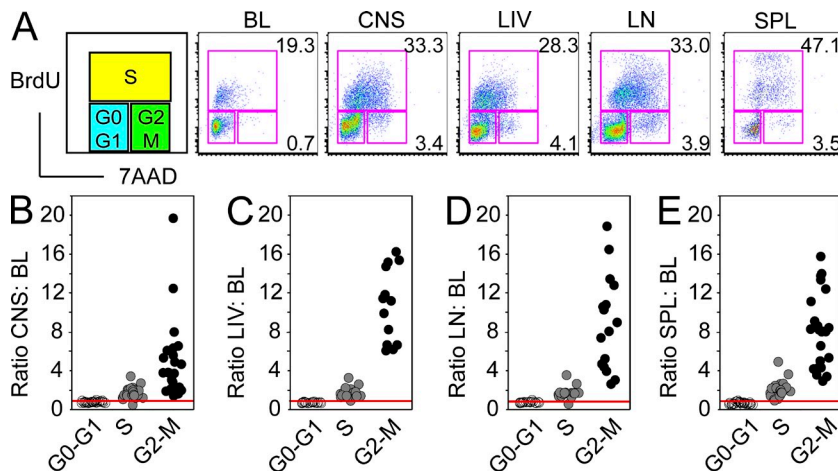
Figure 1. Virus-specific CTLs divide in lymphoid and nonlymphoid sites. To determine the cell cycle stage of virus-specific CTL, blood (BL), CNS, liver (LIV), cervical LNs, and spleen (SPL) of mice seeded with Thy1.1$^+$ P14 cells were harvested 15 min after i.p. BrdU administration on day 6 after LCMV infection. (A) Representative flow cytometric plots of BrdU versus 7AAD are shown for Thy1.1$^+$ P14 cells extracted from tissues of infected mice. (B–E) The ratio of Thy1.1$^+$ P14 cells found in G0-G1, S, or G2-M stages of cell cycle in the CNS (B), liver (C), LN (D), or spleen (E) relative to the blood was calculated for individual mice (n = 16–24 mice per group). Data were compiled from six independent experiments. The red line is set at a ratio of 1 and indicates no difference relative to the blood. The ratio of cells in S or G2-M compared with G0-G1 was significantly different in all tissues examined (P < 0.05, one way ANOVA).

swarms develop and, >24 h later, examples of division are observed with CD4$^+$ T cells abruptly arresting and undergoing cytokinesis within 15 min (Miller et al., 2004). Integration of signals obtained from interactions with multiple APCs, or successive antigen encounters, was also shown to enhance CD4$^+$ T cell differentiation and cytokine production (Gunzer et al., 2000; Bajénoff et al., 2002; Faroudi et al., 2003; Celli et al., 2005). Although initial priming of CD4$^+$ T cell allows division to occur in an antigen-independent manner for several rounds of division, proliferation will eventually stop and requires further peptide-specific interactions to reinitiate the effector CD4$^+$ T cell cycle (Bajénoff et al., 2002). Additionally, in models of experimental autoimmune encephalomyelitis, local CD4$^+$ T cell restimulation in the tissue is required to reactivate the cells and generate effector functions (Flügel et al., 2001; Kawakami et al., 2004, 2005; Bartholomäus et al., 2009). Enhanced CD4$^+$ T cell priming and effector function is therefore reliant on numerous peptide–MHC II interactions that are acquired during initial activation and upon entry into peripheral tissues. It is presently unknown whether integration of multiple peptide–MHC I interactions can modulate CD8$^+$ T cell division programming during the effector stages of an active viral infection. This mechanism would enable infected tissues to control CTL numbers locally and thereby limit immunopathology.

Control of CTL division is of particular importance in the virally infected central nervous system (CNS), an immunologically specialized site (Engelhardt and Ransohoff, 2005) which requires the counterbalance of local immunity against protection of postmitotic cells such as neurons. During an acute viral infection, it is unknown whether CTLs within the CNS retain their proliferative capacities and can be influenced by the local milieu. In general, little is known about CNS CTL division. Although CNS CD8$^+$ T cell division was suggested in vitro and in vivo (Ling et al., 2006, 2008; Wilson et al., 2009), it is unclear whether these data represent proliferation before entry into the CNS (i.e., during migration to the site), cells that are blocked at early stages of cell cycle, or in vitro artifacts caused by responses to mechanical damage in
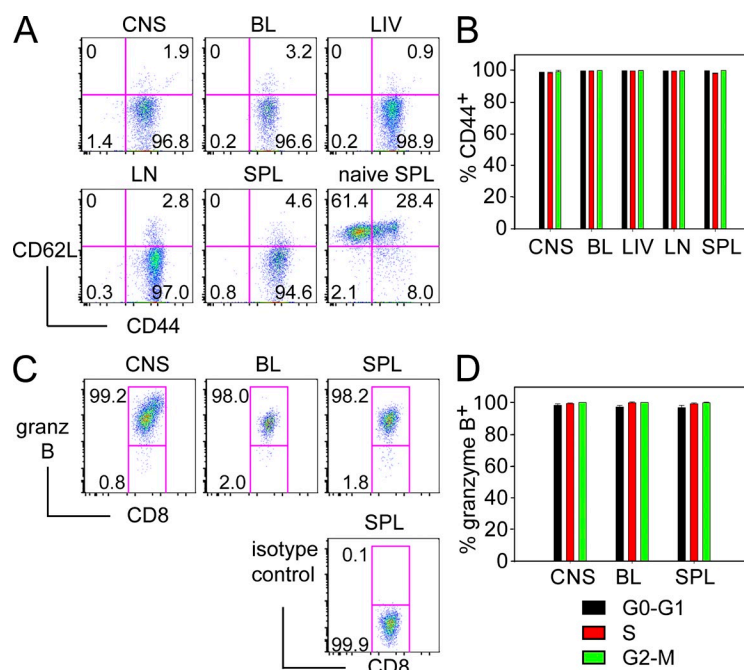
brain tissue (Xu et al., 2007). In this study, we set out to address whether CTL division programming is completely hardwired (i.e., can occur independent of additional interactions) or can in fact be modulated by peptide–MHC I interactions at sites of viral infection. We demonstrate that CTLs remain in cell cycle while transiting through the blood and can undergo cytokinesis within 15 min of arrest in the virally infected meninges. Importantly, we also show that the CTL program is not completely hardwired but is likely cumulative and can be modulated by peptide–MHC I–dependent interactions. These results suggest that CTLs integrate signals from both lymphoid and nonlymphoid tissues to shape their overall proliferative responses.

RESULTS
Virus-specific CTLs migrate in active stages of cell cycle
Initial cognate peptide–MHC I interactions are thought to prime CD8$^+$ T cells and generate a cell division program. Continued cell cycle progression can then occur in a peptide–MHC I–autonomous manner, with division occurring in the absence of further TCR–MHC I interactions (van Stipdonk et al., 2001, 2003). CTL programming may therefore allow continued cell cycle progression to occur in locations that are not ideally suited for division as a result of the lack of antigen or absence of suitable APCs. During viral infection, there is a large expansion of virus-specific cells that occurs within the secondary lymphoid organs (Masopust et al., 2007); however, it is unknown whether significant cell cycle progression occurs during migration to peripherally infected sites. We therefore used the lymphocytic choriomeningitis virus (LCMV) model system to determine if CTL cell cycle progression occurs during migration from lymphoid organs and locally within infected tissues during acute infection.

To study a traceable representative of the CTL response, mice were seeded with 10^4 naive Thy1.1$^+$ P14 CD8$^+$ T cell receptor transgenic cells specific for the D^{b}GP$_{33-41}$ LCMV epitope (Pircher et al., 1989) and were then infected intracerebrally (i.c.) with 10^3 PFU LCMV Armstrong (Arm) to induce

Figure 2. Virus–specific CTLs in cell cycle are activated effector cells. To determine whether the CD8^{+} T cells undergoing cell division in the CNS were naive or activated effectors, the CNS, liver (LIV), blood (BL), cervical LNs, and spleen (SPL) of mice seeded with Thy1.1^{+} P14 cells were harvested 15 min after i.p. BrdU administration on day 6 after LCMV infection. (A) Representative flow cytometric plots of CD44 versus CD62L for Thy1.1^{+} P14 cells. Note the absence of naive P14 cells (identified as CD62L^{+} CD44^{−}) in the tissues of infected animals. (B) Quantification of CD44 expression on P14 cells at all stages of cell cycle. Data are plotted as mean ± SD and are representative of $n = 14$ mice per group collected over four independent experiments. (C) Representative flow cytometric plots of granzyme B or isotype control staining versus CD8 for Thy1.1^{+} P14 cells. (D) Granzyme B expression was quantified in P14 cells at all stages of cell cycle. Data are plotted as mean ± SD and are representative of $n = 19$ mice per group acquired from five independent experiments.

viral meningitis (Kang and McGavern, 2008). During this acute model, CD8^{+} T cells are primed in peripheral lymphoid tissues and then migrate to the CNS on day 6 after infection, at which point the mice develop seizure and succumb to disease (Kang and McGavern, 2008). On day 6 after infection, mice were pulsed i.p. for 15 min with BrdU. The short in vivo BrdU pulse limited the amount of time peripherally labeled CTL had to enter the CNS while still allowing for delineation of specific cell cycle stages (Dean et al., 1984). After the BrdU pulse, mononuclear cells were isolated from the blood, perfused CNS, liver, LNs, and spleen. Strikingly, we observed by flow cytometry that up to a third of Thy1.1[+] P14 CTLs in the blood, CNS, and liver were in active stages (S and G2–M) of cell cycle (Fig. 1 A) with percentages comparable to those observed in the lymphoid organs. The frequencies of cycling virus-specific CTL in blood, CNS, and liver are likely even higher because the G1 stage cannot be distinguished from G0 using this methodology. To determine whether the LCMV-infected nonlymphoid tissues influenced P14 CTL cell cycle progression, we calculated frequencies of CTL in all stages of cell cycle in the CNS (Fig. 1 B) and liver (Fig. 1 C) relative to the blood and compared them to the LNs (Fig. 1 D) and spleen (Fig. 1 E) in each individual animal. We noted a statistically significant increase (P < 0.05) in the percentage of CNS- and liver-infiltrating P14 CTL in the S and G2–M stages of cell cycle, and this trend was comparable to that observed in the LNs and spleen. To demonstrate that our findings were not unique to the LCMV system, we seeded Ly5.1^{+} mice with 10^4 naive Ly5.2^{+} OT-I CD8^{+} T cells and then infected i.v. with 10^6 PFU of vesicular stomatitis virus (VSV) expressing OVA (VSV-OVA) to model a peripheral infection (Fig. S1). At day 5 after infection, mice were pulsed with BrdU for 15 min. Similar to our previous results, up to a third of

Ly5.1[+] OT-I CTLs isolated from the blood, liver, and spleen were found in active stages of cell cycle (Fig. S1 A), and the frequency of CTLs in later stages of cell cycle (G2–M) was significantly increased (P < 0.05) in liver and spleen relative to blood (Fig. S1 B). These data indicate that virus-specific CTLs remain in cell cycle as they migrate through circulation and are therefore poised to complete their cell cycle program upon entry into virally infected tissues such as the CNS and liver.

To ensure that we were examining the continuation of the effector CTL division program rather than initiation of priming within these different sites, the activation status of the virus-specific CD8^{+} T cells was examined. Mice seeded with naive Thy1.1^{+} P14 CD8^{+} T cells were infected i.c. with 10^3 PFU LCMV Arm. On day 6 after infection, animals were pulsed with BrdU and virus-specific cells isolated from the blood, CNS, liver, cervical LNs, and spleen were analyzed for CD44, CD62L, and cell cycle progression. Importantly, P14 cells in all stages of cell cycle were CD44^{hi}, indicating that these cells represented an effector population (Fig. 2, A and B). Granzyme B staining was performed as another assay to ensure that the P14 CTLs under investigation were activated effector cells. Virus-specific P14 CTLs extracted from the blood, CNS, and spleen on day 6 after infection all expressed granzyme B regardless of the cell cycle stage (Fig. 2, C and D). These data demonstrate that the CTLs observed cycling in blood, lymphoid tissues (spleen and LN), and nonlymphoid tissues (CNS and liver) were bona fide effector cells and not naive precursors.

CTL division occurs in the CNS and is preceded by cellular arrest

To gain novel insights into the anatomy and dynamics of CTL division at an active site of viral infection, we focused on the LCMV-infected meninges at day 6 after i.c. inoculation. This anatomical region was selected for three reasons. First, it remains controversial as to whether CTLs actively divide in the CNS. Second, the LCMV-infected meninges contain an

abundance of CTL at this time point, making it convenient to study CTL–target cell interactions during a relevant model of disease. Third, the meninges can be visualized through a surgically thinned skull with a two-photon microscope (Kim et al., 2009; Yang et al., 2010), allowing for real-time analysis of CTL division events in a physiological setting. To provide definitive evidence of CNS CTL proliferation, we first set out to define the anatomical localization of CTL division events. This was accomplished using static and dynamic imaging approaches. Confocal analyses were performed on 6-µm frozen brain sections from day-6 mice seeded with GFP-tagged P14 cells (McGavern et al., 2002). Tissues were stained with Ki-67 to mark proliferating cells in all stages. Clear examples of Ki-67$^+$ GFP$^+$ P14 cells captured during cytokinesis, the last stage of division, were detected within the CNS meningeal space (Fig. 3). Quantification of Ki-67$^+$ cells in the meningeal space versus the parenchyma revealed that the majority of cycling cells were found in the meninges (142/464 cells [30%] in the meninges vs. 3/85 cells [3.5%] in the parenchyma), suggesting that this space is more permissive for T cell division. This is likely a result of the fact that LCMV infection and infiltrating APCs are mostly confined to the meningeal space in this model (Kim et al., 2009). Together, these data clearly demonstrate that CTL division can occur within the CNS environment.

To examine the dynamics of CNS CTL division, we performed two-photon laser-scanning microscopy through a thinned cranial window (Xu et al., 2007; Yang et al., 2010) in mice at day 6 after infection (Fig. 4; Fig. S2; and Videos 1 and 2).
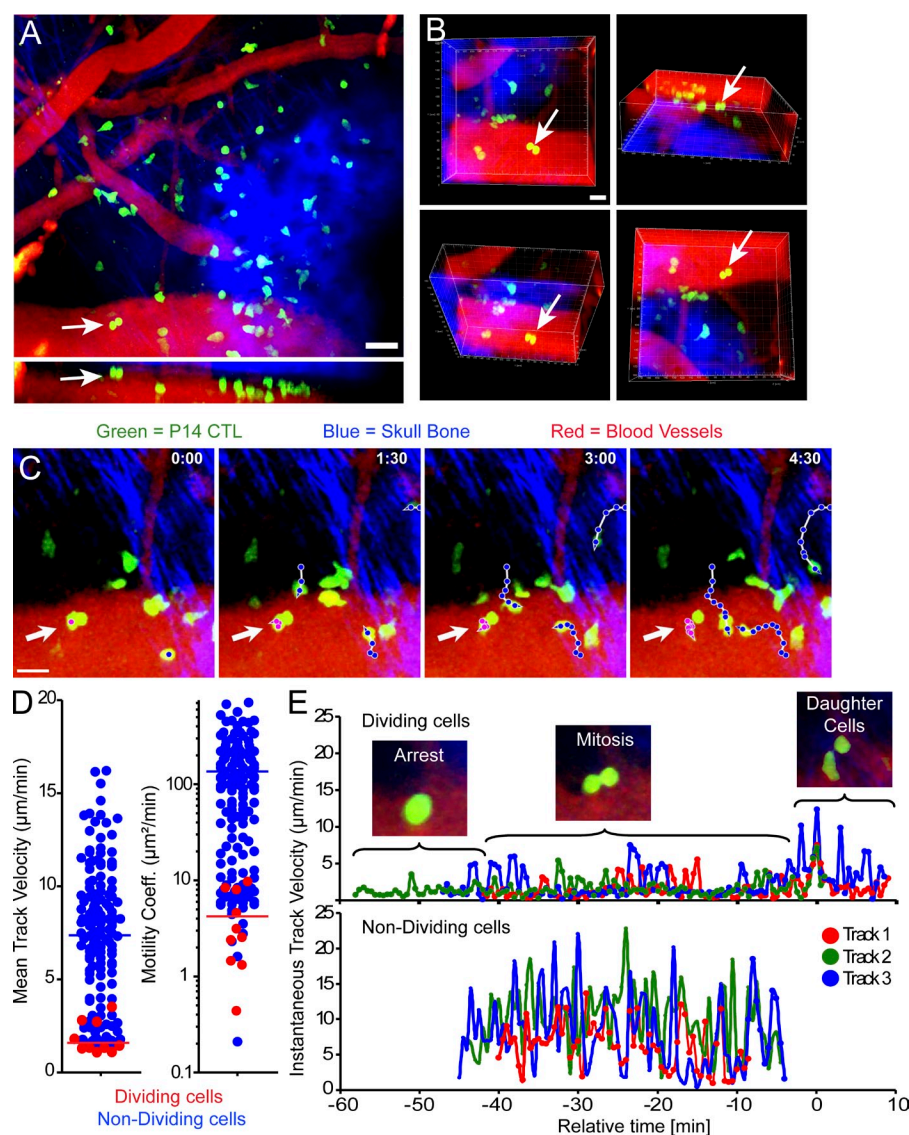
This enabled us to evaluate the position and timing of CTL division within the meningeal space. Importantly, this technique also allowed us to visualize CTL dynamics in the undisrupted CNS, thus avoiding potential artifacts induced by mechanical tissue damage. We focused exclusively on the final phase of cell division (mitosis/cytokinesis) because this could be easily observed and quantified. Visual analyses of 4D time lapses spanning 30–60 min revealed that 1.4% of P14 CTL (11/788 cells) underwent mitosis in the meninges (Fig. 4; and Fig. S2, A and B). The cells were normally found beneath the skull bone, mostly above the brain parenchyma, and outside of meningeal blood vessels (Fig. 4, A and B; and Video 2), although division within a blood vessel was observed occasionally (Fig. S2 C; and Video 1, example 3). Quantitative analyses of CTL division revealed that mitosis was usually preceded by cell arrest, as indicated by low mean track velocities, instantaneous track velocities, and motility coefficients (Fig. 4, C–E). Dividing CTL did not become fully motile again until daughter cells were generated (Fig. 4 E). Interestingly, we observed that after deceleration and arrest, GFP$^+$ P14 CTL could undergo mitosis within just 10–15 min (Fig. S2, A and B; and Video 1, examples 1 and 2). Division occurring within minutes of arrest, rather than the estimated hours described for naive T cell priming in lymphoid organs (Murali-Krishna et al., 1998), supports the idea that many CTLs arrive at sites of infection in active stages of cell cycle and then receive additional instruction regarding whether to divide or not.
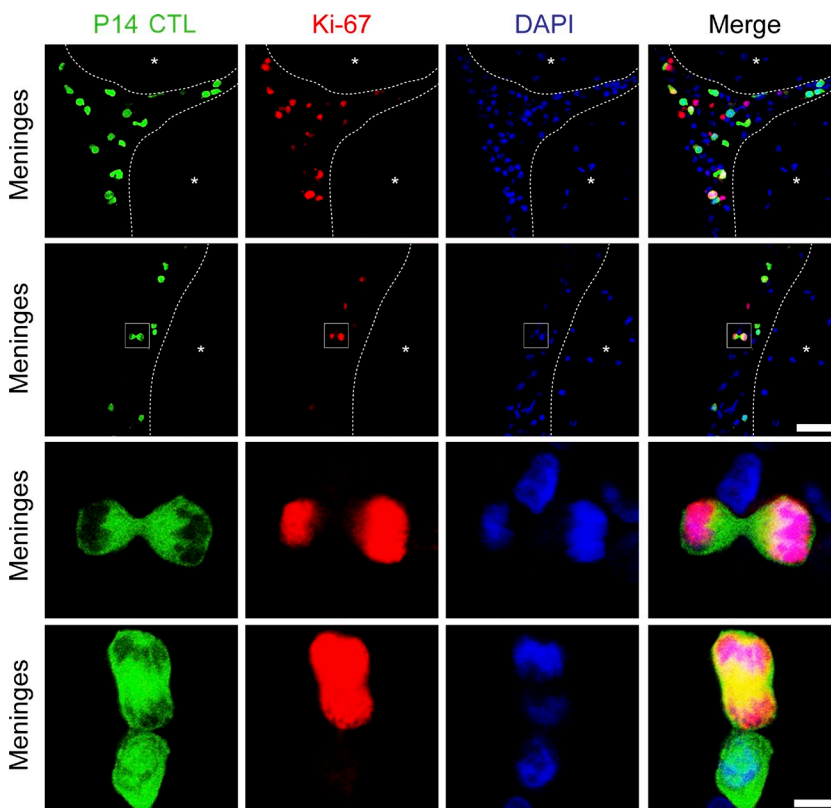
Cognate peptide–MHC I interactions modify the CTL division program

We have shown previously that direct injection of anti–MHC I into the subarachnoid space elevates the motility of all GFP$^+$ P14 cells in the meninges at day 6 after

Figure 3.   Virus-specific CTLs divide in the meninges of the CNS. To examine whether virus-specific CTLs divided locally within the CNS, brains from mice seeded with GFP$^+$P14 cells and then infected i.c. with 10^3 PFU LCMV Arm were harvested on day 6 after infection. Frozen sections were cut and stained with Ki-67 (red) to detect dividing CNS-infiltrating GFP$^+$ P14 cells (green). Shown are representative panels to reflect anatomical location and division events. The top two rows show lower magnification images and the dashed lines represent the border between the meninges and brain parenchyma. Bar, 30 µm. The asterisks denote the parenchymal portion of the tissue. The white boxes in the second row highlight a mitotic CTL that is enlarged in the third row. Both the third and fourth rows show representative examples of individual virus-specific P14 cells undergoing mitosis within the meningeal space. Bar, 5 µm. Cell nuclei were counterstained with DAPI (blue). Data are representative of two independent experiments (n = 8 mice).

Figure 4. **Anatomy and dynamics of virus–specific CTL division in the CNS.** (A) A representative maximal projection of a 3D z-stack is shown for a mouse at day 6 after infection. The projection represents one time point in a 51-min film. The white arrows denote a GFP+ P14 CTL undergoing mitosis (See Video 2). The strip beneath the maximal projection shows a view through z-stack at the position of the dividing cell (arrow). Note that the dividing cell is positioned in the meninges above a blood vessel (red) and beneath the skull bone (blue). (B) A cropped area is shown depicting the dividing CTL in A. Different 3D projections were generated by rotating the z-stack around the x axis. The dividing CTL is always denoted with an arrow. Bars, 20 µm. (C) A representative time lapse is shown for a P14 CTL (green) dividing in the meninges (arrow; see Video 2). The magenta track shows the position of the dividing CTL at each point in the time lapse. Note that the CTL is stationary when compared with three motile nondividing CTLs (blue tracks). (D) The mean track velocity and motility coefficient were calculated for dividing (red) and nondividing (blue) P14 CTLs in the meninges. Means are denoted by horizontal bars. (E) Instantaneous track velocities are plotted versus time for three representative dividing (top graph) and nondividing (bottom graph) P14 CTLs. Brackets in the top graph denote velocities in three phases of CTL division: arrest, mitosis, and the split into two daughter cells. Data are representative of five independent experiments ($n = 13$ mice).

infection, indicating that MHC I interactions influence the dynamics of most (if not all) CTLs in the CNS environment (Kim et al., 2009). Because our two–photon data revealed that P14 CTL division was preceded by cell arrest (Fig. 4, Fig. S2 B, and Videos 1 and 2), we hypothesized that advancement through the division program at sites of infection was dependent in part on cognate peptide–MHC I interactions. To test this theory, we first isolated and phenotypically examined CNS APCs at day 6 after infection (Fig. 5, A and B) to determine if there were cells that could potentially stimulate virus–specific CTL. In both mock and day 6–infected animals, the CD11b+ CD45.2lo resident microglia population was detected; however, infiltrating macrophage/monocytes (CD11b+ CD45.2hi CD11c−) and DCs (CD11b+ CD45.2hi CD11c+) were only detected upon infection (Fig. 5 A). Analysis of surface MHC I, MHC II, CD80, and CD86 levels on day 6 after infection demonstrated that DCs and macrophage/monocytes recruited from the periphery have a higher stimulatory potential

compared with microglia as a result of their enhanced levels of MHC I and costimulatory molecules (Fig. 5 B). To determine which CNS APC populations (if any) contained LCMV antigen and, thus, the potential to present cognate peptide to infiltrating P14 CTL, we generated a three-segment LCMV recombinant that expresses teal fluorescent protein (r3LCMV-TFP) and then flow cytometrically analyzed TFP expression in CNS cells at day 6 after infection (Fig. S3). Approximately 1–2% of DCs, macrophages/monocytes, and microglia were TFP+ in symptomatic mice at day 6. However, the majority of TFP expression was found in stromal cells (CD45.2− gp38+), which were demonstrated previously to be a primary target for LCMV in the meninges (Kim et al., 2009). Collectively, these data demonstrate that multiple meningeal cell populations have the potential to be engaged by P14 CTL during meningitis.

Although programming instituted in lymphoid tissues can set cell cycle into motion, we postulated that local tissue interactions with APCs could further influence cell cycle progression. To determine whether CNS APCs displaying cognate peptide–MHC I complexes could impact cell cycle,
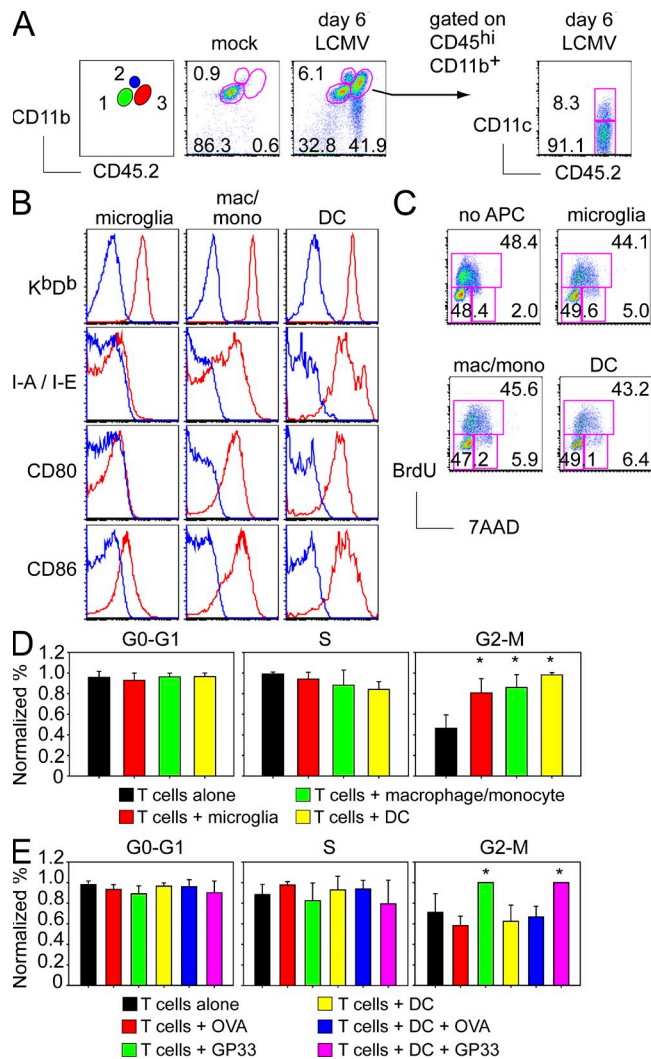
Figure 5. Peptide–MHC I interactions influence the division program of virus–specific CTL. (A) Representative flow cytometric plots depict the non–T cell component of CNS mononuclear cells in mock versus day-6 LCMV-infected mice. Plots are gated on Thy1.2-negative cells. The schematic plot on the far left shows the relative position of 1, microglia; 2, neutrophils; and 3, macrophages/monocytes/DCs. To further delineate macrophages/monocytes and DCs, the cells in region 3 were subdivided into CD11c$^-$ CD45.2^{hi} CD11b$^+$ (macrophages/monocytes) and CD11c$^+$ CD45.2^{hi} CD11b$^+$ (DCs) as shown in the far right plot. Data are representative of n = 16–24 mice per group accumulated over four to six experiments. (B) Representative histograms show the expression of MHC class I (K^{b}D^b), MHC class II (I-A/I-E), CD80, and CD86 (red) relative to isotype controls (blue) on microglia (Thy1.2$^-$ CD45.2^{lo} CD11b$^+$), macrophages/monocytes (Thy1.2$^-$ CD45.2^{hi} CD11b$^+$ CD11c$^-$), and DCs (Thy1.2$^-$ CD45.2^{hi} CD11b$^+$ CD11c$^+$) at day 6 after infection. Data are representative of n = 16 mice collected in three separate experiments. (C) Sorted effector virus-specific CTL pooled from four mice were stimulated at a 2:1 ratio with sorted GP33 peptide-pulsed CNS APCs isolated from day 6–infected animals (n = 20). BrdU was added to the in vitro culture for the last 30 min of the 90-min incubation. Representative BrdU versus 7AAD staining of CD8$^+$ Thy1.1$^+$ P14 cells incubated alone or with CNS APCs is shown. These data are representative of four separate experiments. (D) Normalized percentages of T cells in various stages of cell cycle are shown. Data

we harvested cells from the CNS, pulsed them with GP$_{33-41}$ peptide, and flow cytometrically sorted microglia, macrophage/monocytes, and DCs from day 6–infected mice. In parallel, P14 CTLs were sorted from the spleens of day-6 LCMV Arm–infected Thy1.1$^+$P14 seeded animals. The sorted resident and infiltrating CNS APCs were then incubated with P14 CTL for 1.5 h in vitro, pulsed with BrdU, and the T cells were assessed for their BrdU versus 7AAD profile. Interestingly, microglia, macrophage/monocytes, and DCs were all able to significantly increase (P < 0.001) the frequency of P14 CTL in the final G2-M stage of cell cycle (Fig. 5, C and D). Moreover, infiltrating DCs had a slightly higher capacity to advance cell cycle progression than tissue-resident microglia (P < 0.05). Therefore, both resident and infiltrating CNS APCs have the potential to modulate virus-specific effector CTL division during viral infection.

To determine whether the modification in cell cycle progression involved cognate peptide–MHC I interactions, the peptide specificity of the response was examined. As a result of the inherently difficult nature of isolating sufficient numbers of cells from the CNS, splenic DCs were used to stimulate P14 CTL. The ability to increase the frequency of CTL in G2-M was reproduced using splenic DCs (Fig. 5 E). Sorted splenic DCs from LCMV Arm–infected animals were incubated with sorted P14 CTL for 1.5 h in vitro in the presence of either GP$_{33-41}$ peptide or an irrelevant peptide (OVA$_{257-264}$). Interestingly, incubation of P14 CTL (in the presence or absence of DCs) with GP$_{33-41}$ peptide significantly increased (P < 0.05) the percentage of cells in G2-M (Fig. 5 E). In contrast, addition of OVA$_{257-264}$ had no impact on cell cycle. That GP$_{33-41}$ peptide–pulsed T cells alone showed increased frequencies of P14 CTL in G2-M is likely a result of presentation of peptide by T cell MHC I. These in vitro data indicate that cognate peptide–MHC I interactions can influence the cell cycle program in virus-specific CTL regardless of whether the peptides are displayed on professional APCs or not.

We next sought to determine if local APCs and cognate peptide–MHC I interactions influenced the CTL division program in vivo. To do this, we first examined the degree to which P14 CTL division was associated with engagement of professional APCs (i.e., DCs) in the CNS. This was accomplished by seeding CD11c-YFP reporter mice (Lindquist et al., 2004) with CFP$^+$ P14 cells and examining interactions in the meninges by two-photon microscopy at day 6. We observed multiple examples of P14 CTL clustering around CD11c-YFP$^+$ DCs in the meninges and dividing either during or after

were normalized from four independent experiments. (*, P < 0.05, one-way ANOVA). (E) Sorted effector Thy1.1$^+$ P14 cells pooled from two to four mice were stimulated at a 2:1 ratio with splenic DCs isolated from day 6–infected animals (n = 2–3) in the presence of OVA or GP33 peptide. The BrdU incubation is the same as in C. Normalized percentages of T cells in various stages of cell cycle are shown (*, P < 0.05, one way ANOVA). These results are compiled from three independent experiments. Data in D and E are plotted as mean ± SD.
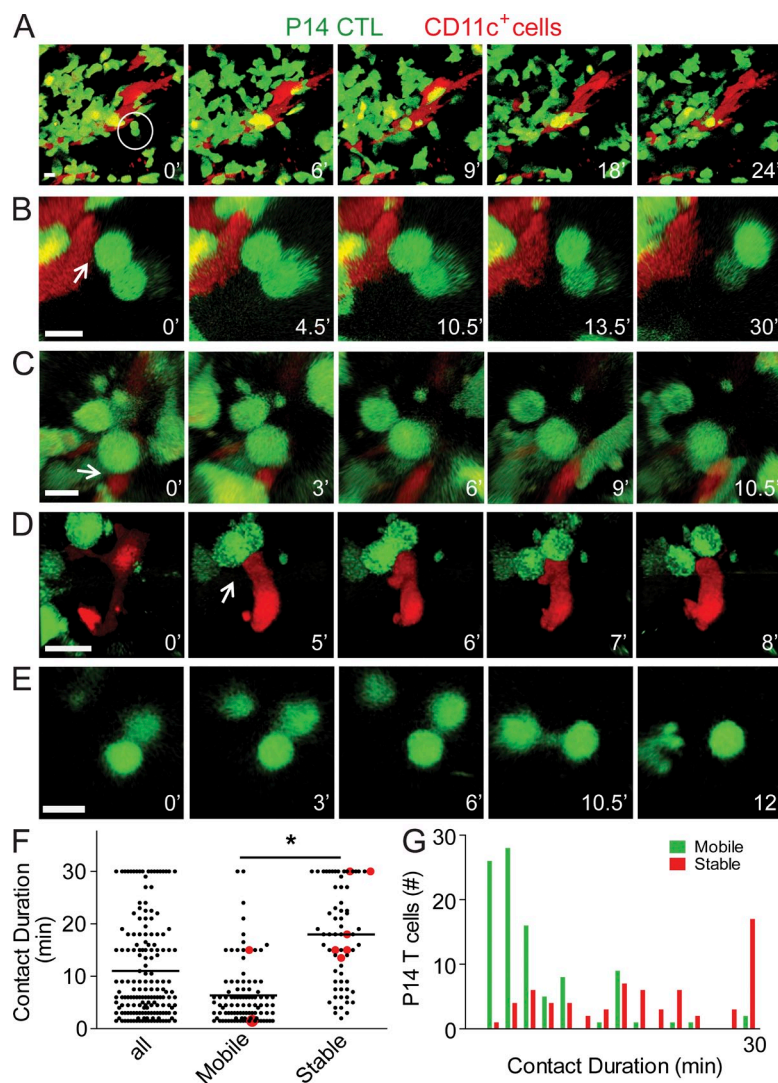
Figure 6. CTLs form stable and dynamic contacts with DCs during LCMV meningitis. (A–E) Representative time lapses of 3D reconstructions show the position of dividing CFP⁺ P14 CTL (green) in relation to CD11c-YFP⁺ DCs (red) in the meninges at day 6 after infection (see Video 3). Panel A shows CTL swarming around and contacting a large YFP⁺ meningeal DC. One P14 CTL (circle) divides after contact with this DC. An enlarged view of the dividing cell, as well as the CTL-DC contact point (arrow), is shown in B. C and D show two additional examples of CTL mitosis after DC contact (arrows), whereas E illustrates a P14 CTL that divides when not in contact with a DC. Bars, 10 μm. (F) Contact durations (in minutes) between P14 CTL and meningeal DCs were calculated from 30-min time lapses. Contacts were divided into two categories with respect to YFP⁺ DCs: mobile contact (>2 μm/min) and stable contact (≤2 μm/min). Each dot represents an individual P14 CTL. Red dots denote P14 CTL that divided while contacting YFP⁺ DCs. The mean ± SD contact durations were 11.0 ± 9.3 min (all), 6.3 ± 5.9 min (mobile), and 17.9 ± 9.3 min (stable). Asterisk denotes a statistically significant (P < 0.00001, Mann-Whitney rank sum test) difference between mobile and stable contacts. Means are denoted by horizontal bars. (G) The frequency of mobile and stable P14 CTL contacts represented as a histogram (bin size = 2 min). Data are compiled from n = 4 mice (nine different fields).

engagement (Fig. 6, A–D; and Video 3). Analysis of P14 CTL motility adjacent to meningeal DCs revealed both mobile cells (moving at >2 μm/min) and stable cells (moving at ≤2 μm/min; Fig. 6, F and G). In general, stable CTLs engaged with DCs for longer contact duration times and were statistically more likely to divide than motile CTLs (Fig. 6 F). However, CTL division was not linked exclusively to DC contact, as examples of CTL division were observed in areas devoid of CD11c-YFP⁺ DCs (Fig. 6 E and Video 3). These data suggest that DCs can promote CTL division but are likely not the only cell population capable of doing so in the infected meninges.

To evaluate the role of cognate peptide–MHC I interactions in modulating the CTL division program in vivo, Thy1.1⁺ P14 effector cells from day 6–infected spleens (which were all CD44^hi CD62L^lo) were transferred i.v. into either LCMV Arm i.c.-infected WT or H-2D^(b−/−) Thy1.2⁺ hosts. D^b GP_{33–41}-restricted P14 CTL transferred into H-2D^(b−/−) mice received no further peptide–MHC I stimulation; however, meningitis proceeded normally in these mice as a result of the intact H-2K^b–restricted CTL response. 90 min after transfer, mice

were pulsed with BrdU in vivo for 15 min and the perfused CNS was harvested. This short time period was used to limit P14 CTL trafficking through multiple tissues. Analysis of cell cycle in CNS-infiltrating Thy1.1⁺ P14 CTL revealed that H-2D^b deletion significantly (P ≤ 0.006) reduced the percentage of cells in S phase, and, consequently, increased the percentage of cells in G0-G1 (Fig. 7, A and B). That we observed an increased percentage of CTL in G2-M (rather than S) in vitro (Fig. 5, D and E) can be explained by the immediate interactions that occur in cultures pulsed with peptide, which likely advance the CTL to a later stage of cell cycle in 90 min. During this same time period in vivo, CTL must circulate through the blood and extravasate into infected tissues before encountering further peptide–MHC complexes. These data indicate that additional MHC I signals received by virus-specific CTL support cell cycle progression in vivo.

Because CNS APCs showed increased expression of CD80/CD86 (Fig. 5 B), and costimulatory molecules can influence naive T cell division (Croft et al., 1994; Salomon and Bluestone, 2001), we examined the influence of these pathways on cell cycle by simultaneously blocking CD80 and CD86 with CTLA-4-Fc (Linsley et al., 1992; Garidou et al., 2009). Thy1.1⁺P14 seeded animals were infected i.c. with 10³ PFU LCMV Arm before administration of PBS or CTLA-4-Fc on days 4 and 5 after infection. Analysis of BrdU incorporation on day 6 after infection revealed that CTLA-4-Fc treatment had no impact on cell cycle for P14 CTL found in the CNS (Fig. 7 C). To ensure that contributions of the CD80/CD86
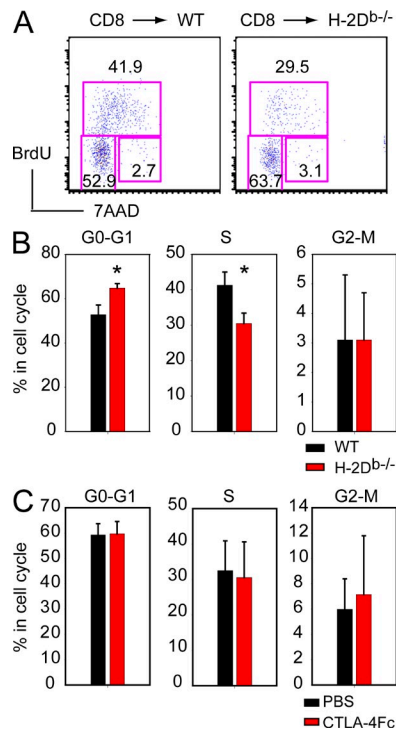
Figure 7. MHC I but not CD80/CD86 expression influences the ability of virus–specific CTL to enter cell cycle in the CNS. (A and B) 3.0×10^7 CD8+ T cells isolated from the spleens of day-6 mice seeded with Thy1.1+ P14 cells were transferred i.v. into day-6 LCMV-infected WT or H-2Db−/− recipients. Approximately $2–3 \times 10^6$ of the transferred cells were CD8+ Thy1.1+ P14 cells. 90 min after adoptive transfer, recipient mice received 2 mg BrdU i.p. and were harvested 15 min later. (A) Representative dot plots of BrdU versus 7AAD staining shown for CD8+ Thy1.1+ P14 cells that infiltrated the CNS of recipient mice. (B) The percentage of CD8+ Thy1.1+ P14 cells in G0-G1, S, and G2-M is shown for WT or H2Db−/− mice. Data are shown as mean ± SD for a single experiment and are representative of $n = 14$ mice per group collected over four independent experiments. The asterisk denotes statistical significance (P ≤ 0.006, Student's t test). (C) To block CD80 and CD86, WT B6 mice seeded with Thy1.1+ P14 cells were injected i.p. on days 4 and 5 after LCMV infection with 200 µg CTLA-4-Fc (red) or PBS (black). The percentage of CNS Thy1.1+ P14 cells (mean ± SD for a single experiment) in the denoted stages of cell cycle was analyzed at day 6 after infection. Data are representative of $n = 22–24$ mice per group acquired over six independent experiments.
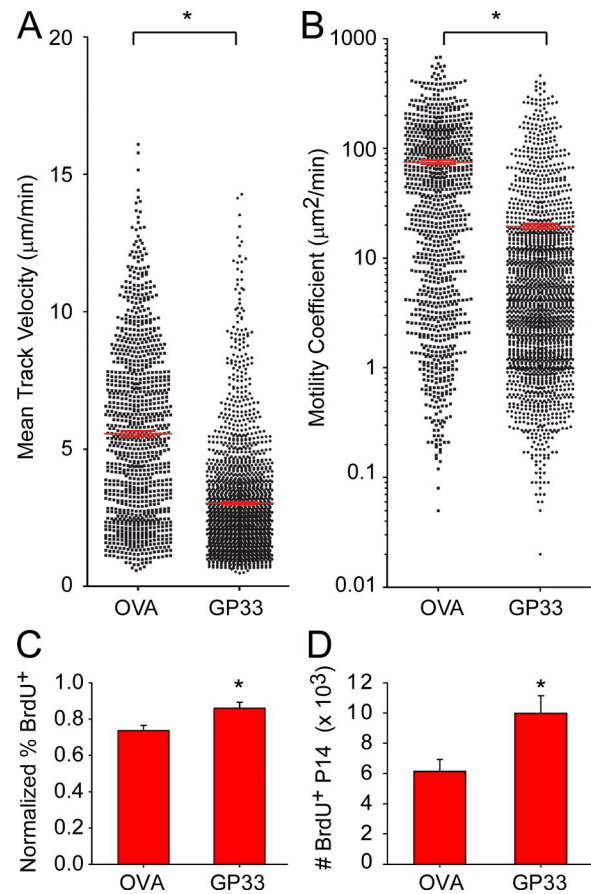

Figure 8. Cognate peptide interactions increase CTL division in the meninges. P14 CTL motility and division were examined after administration of cognate (GP$_{33-41}$) or irrelevant (OVA$_{257-264}$) peptide into the subarachnoid space of P14 seeded mice at day 6 after infection. Mean track velocities (A) and motility coefficients (B) were calculated for GFP+ P14 CTL imaged in the meninges within the first hour after peptide administration. (*, P < 0.001, Mann-Whitney rank sum test). Each dot represents an individual P14 CTL quantified from mice receiving GP33 ($n = 1,888$ tracks, $n = 11$ mice) or OVA ($n = 1,016$ tracks, $n = 8$ mice). Data are compiled from six to eight independent experiments. Red line denotes the mean ± SEM for each group. The normalized frequency (C) and absolute number (D) of BrdU+ Thy1.1+ P14 CTL were calculated 90 min after administration of BrdU and peptide into the subarachnoid space. (*, P < 0.05, Student's t test). Data are plotted as mean ± SEM and are representative of 15–16 mice compiled over four independent experiments.

costimulation pathways were not being overlooked as a result of potential limitations in the ability of the CTLA-4-Fc molecule to cross the blood brain barrier, we also examined another peripheral site of infection (liver). Similar to the brain, cell cycle analysis of P14 CTL derived from the liver also showed no significant changes in cell cycle upon CTLA-4-Fc treatment (unpublished data). Collectively, these data indicate that MHC I interactions can directly influence the cell cycle program of antiviral CTL in vivo, whereas CD28-dependent costimulation is dispensable.

Our studies performed in H-D$^{b−/−}$ mice support the concept that peptide–MHC I interactions facilitate CTL division in vivo. To provide additional support for this concept,

we conducted a complementary line of investigation that involved administration of cognate peptide directly into the subarachnoid space (Fig. 8). Mice were seeded with Thy1.1+ or GFP+ P14 cells and then infected with LCMV i.c. At day 6 after infection, a small craniotomy was performed and cognate (GP$_{33-41}$) or an irrelevant (OVA$_{257-264}$) peptide was administered into the subarachnoid space for 90 min. To determine the impact on CTL dynamics, we examined the motility of GFP+ P14 cells by two-photon microscopy within the first hour of peptide administration. As expected, injection of cognate peptide significantly decreased (P < 0.001) both the mean velocity and motility coefficient of GFP+ P14 CTL. Within

the meningeal space of mice treated with GP$_{33-41}$, the majority of P14 CTLs were found to be arrested (Fig. 8 A). To determine whether enhanced cognate peptide–MHC I interactions influenced CTL division, we administered BrdU into the subarachnoid space during the peptide incubation period. The results of this experiment revealed that a short 90-min exposure to GP$_{33-41}$ peptide significantly increased (P = 0.008) both the frequency and absolute number of BrdU$^+$ P14 CTL in the brain (Fig. 8, C and D). These data indicate that cognate peptide–MHC I interactions can indeed influence CTL division programming.

DISCUSSION

The importance of the T cell division program in determining the magnitude and efficiency of the antiviral response is widely accepted (van Heijst et al., 2009). In this study, we examined whether the antiviral CTL division program proceeds after departure from lymphoid tissues and whether this program can be influenced by cognate peptide–MHC I interactions at sites of viral infection. A modifiable, rather than completely hardwired, division program would give infected tissues the ability to control CTL numbers locally to either improve the efficiency of viral clearance or limit unwanted immunopathology. Importantly, we observed in two different viral model systems that antiviral CTLs circulate through the blood in active phases of cell cycle (primarily S phase) and could even, on occasion, undergo cytokinesis in meningeal vasculature. Within the virus-infected meninges, we definitively demonstrated, using two-photon microscopy, that the CNS is a permissive site for CTL division. CTL mitosis/cytokinesis is normally associated with stable interactions, and division could occur within 10–15 min of CTL arrest. Moreover, at the peak of viral meningitis, approximately one third of CTLs extracted from the CNS were in active stages of cell cycle, which was comparable to what was observed in peripheral tissues such as the liver, cervical LNs, and spleen. These data suggest that the CTL division program is not completely hardwired but rather can proceed in transit and be influenced at sites of active viral replication. In support of this concept, we provided evidence both in vitro and in vivo that peptide–MHC I interactions could modulate the CTL division program.

We propose that control of viral dissemination versus prevention of unwanted immunopathology can be balanced in part through local modulation of CTL division programming. Previous studies have shown that T cell division is a relatively slow process that occurs on the order of hours (Murali-Krishna et al., 1998; Veiga-Fernandes et al., 2000). In addition, initial priming events are thought to impart a cellular division program in CD8$^+$ and CD4$^+$ T cells that can later become independent of TCR–MHC interactions (van Stipdonk et al., 2001, 2003; Bajénoff et al., 2002). The initiation of this program in secondary lymphoid tissues could explain the relatively high frequency of CTL we observed cycling in the blood. In fact, 20% of P14 CTLs in the blood were found in S phase, indicating that division is not accomplished solely in solid lymphoid and nonlymphoid tissues but can occur during T cell migration throughout the body. These data combined with

our two-photon imaging studies verify that the blood is a viable site for the continuation of cell cycle. Relative to the blood, we also observed an enhanced frequency of CNS and liver-infiltrating CTL in the S and G2-M phases of cell cycle, which was comparable to that observed in secondary lymphoid tissues. These data suggest that CTL can progress through cell cycle upon arrival in nonlymphoid sites of viral infection. It is important to note that in all of these studies, we pulsed animals in vivo for only 15 min with BrdU (an extremely limited time frame) to capture events that occurred in the tissue under investigation. This enabled us to avoid studying CTL division events that transpired in other sites before arrival in the blood or nonlymphoid tissues.

Upon CTL entry into the brain, it is unclear which anatomical regions (if any) fully support CD8$^+$ T cell division. In vitro studies have shown that naive OVA-specific CD8$^+$ T cells could divide after being added to an organotypic brain slice culture previously injected with OVA (Ling et al., 2008). These data suggest that naive CD8$^+$ T cells might have the capacity to be primed and divide in the brain parenchyma under more physiological circumstances. However, this conclusion was called into question by a more recent study demonstrating that CTL division in brain slices from *Toxoplasma gondii*–infected mice was an extremely rare event and was observed in only 2 of 10,000 cells imaged by two-photon microscopy (Wilson et al., 2009). In our studies, we used multiple approaches to prove that CNS CTL division occurs in vivo after an acute viral infection. Our flow cytometric studies demonstrated that one third of CNS-infiltrating P14 CTLs were in active stages of cell cycle (S or G2-M). This finding was confirmed by confocal microscopic analyses, which revealed that 30% of P14 CTLs were Ki-67$^+$ in the meninges, whereas only 3.5% were positive in the brain parenchyma. These data indicate that the meninges are a more permissive site for CTL division in this model system. This is likely a result of the fact that viral antigen is restricted primarily to the meninges after intracerebral LCMV inoculation; however, it is also conceivable that the brain parenchyma is less permissive of CTL division, as suggested in the *T. gondii* study (Wilson et al., 2009).

Although priming events can impart a differentiation and division program in naive T cells that is antigen independent (or hardwired), we have demonstrated both in vitro and in vivo that the CTL proliferative response can be modulated by cognate peptide–MHC I interactions. In fact, one of the most interesting findings in our study emerged from videos of P14 CTL undergoing mitosis/cytokinesis in the virally infected meninges. Our results revealed that CTL mitosis was usually preceded by cellular arrest and could occur within 15 min of this arrest. These data suggested that the CTL division program was influenced in part by peptide–MHC I interactions and was cumulative in nature. That antiviral CTL can divide within 15 min of arrest in the CNS is reminiscent of late-stage naive CD4$^+$ T cell priming in the LN (Miller et al., 2004). 24 h after first contact with DCs bearing cognate antigen, naive CD4 T cells migrate autonomously, eventually stop, round up, and undergo mitosis/cytokinesis, all within ∼20 min (referred

to as stage V; Miller et al., 2004). Our CTL imaging data suggest that effector cells have the capacity to depart lymphoid tissues during this stage and complete their division program elsewhere. This supposition is consistent with the ability of T cells to integrate signals through multiple transient interactions. In fact, it is well described that CD4^{+} T cells during priming can accumulate signals after interactions with different APCs that allow for differentiation and proliferation (Gunzer et al., 2000; Faroudi et al., 2003; Celli et al., 2005). In vitro, T cells exposed to intermittent signaling were still able to generate IFN-γ responses, indicating that signals can be integrated over time. Additionally, although hardwired programming was sufficient for the first few rounds of CD4^{+} T cell division, secondary waves of proliferation were dependent on reexposure to antigen (Bajénoff et al., 2002).

We previously demonstrated in the LCMV meningitis model that injection of anti–MHC I antibody into the subarachnoid space shifts the velocity distribution for the entire population of meningeal P14 CTL (Kim et al., 2009), suggesting that all P14 cells encountered antigen during the imaging period. Because CTL arrested before undergoing mitosis, we hypothesized that this event might also be linked to cognate peptide–MHC I engagement. This conclusion is supported by our in vitro studies showing that cognate peptide–MHC (but not irrelevant peptide–MHC) interactions modulate CTL cell cycle progression. We also demonstrated in vivo that the absence of MHC I interactions significantly reduced the percentage of CTL in S phase, whereas direct injection of cognate peptide into the subarachnoid space increased the frequency and absolute number of BrdU[+] CTL in the brain. Although peptide–MHC I peptide interactions were important for the enhancement (or maintenance) CTL cell cycle programming, CD28-dependent costimulation was dispensable. Simultaneous blockade of CD80 and CD86 had no impact on CTL cell cycle programming in vivo. Collectively, these data suggest that after departure from lymphoid tissues CTLs continue to integrate proliferative signals obtained from nonlymphoid sites of infection (in this case, the CNS). It is also plausible that serial transient interactions at the site of infection contribute to the overall proliferative program. Programming acquired through transient contacts would be consistent with the fact that most P14 CTLs in the LCMV-infected meninges do not engage in stable long-duration interactions (Kim et al., 2009), as well as with a recent study demonstrating that T cell receptor internalization is not completely dependent on motility arrest or stable immunological synapse formation (Friedman et al., 2010).

Based on our in vitro and in vivo data, the cell populations that support CTL division in the meninges likely include both professional and nonprofessional APCs. Microglia, macrophages, DCs, and stroma were all found to contain LCMV antigen and, thus, had the opportunity to present peptide–MHC I complexes to P14 CTL. Moreover, our in vitro studies demonstrated that display of cognate peptide–MHC I by professional APCs or T cells similarly advanced the CTL division program. In vivo, we observed that CTL clustered around meningeal CD11c^{+} DCs and that division could occur either during or after DC engagement. This observation is consistent with a recent study showing that DCs can support memory CD8 T cell division in sensory dorsal root ganglia latently infected with herpes simplex virus (Wakim et al., 2008). However, CTL division in the LCMV-infected meninges was not linked exclusively to DC contact, as mitotic events were observed in areas devoid of DCs. Thus, although it is clear from our studies that CTL division can be linked to DC contact, it will be important in future studies to identify the other cell populations and molecular mediators that support CTL division in the brain. It will also be important to define the factors that dictate whether a CTL divides or kills after target cell engagement.

In conclusion, our novel findings demonstrate that the division program is not completely hardwired and destined to occur exclusively in lymphoid tissues. Rather, antiviral CTLs remain in cell cycle during migration through the blood and can undergo mitosis within 15 min of arrest in a virally infected tissue. These data suggest that the division program is cumulative and results from the summation of signals received systemically after infection. Departure of CTL from lymphoid tissues while in cell cycle likely gives the host an advantage over the invading pathogen by allowing the response to be modulated as needed at the site of infection. We postulate that this mechanism enables infected tissues to fine-tune the adaptive immune response by applying proliferative brakes to limit unwanted immunopathology or by facilitating cell cycle progression to outcompete increasing viral replication. The latter is important from the standpoint of viral control, as it was recently shown that effector/target cell ratios at the site of infection correlate with whether a pathogen is controlled or not (Li et al., 2009). Our data demonstrate that CTL division can be influenced by cognate peptide–MHC I interactions; however, the degree to which the division program is aborted versus enhanced at the site of infection remains to be determined. If both positive and negative signals can be imposed on the division program locally, then it should be possible to therapeutically modulate CTL at sites of infection to foster clearance while preserving tissue integrity.

MATERIALS AND METHODS

Mice. C57BL/6J (B6), B6.SJL-*Ptprc^a Pepc^b*/BoyJ (Ly5.1 mice), BL/6-Tg(TcraTcrb)1100Mjb/J (OT-I mice), B6 Thy1.1[+]D[b]GP$_{33-41}$ TCR-tg (Thy1.1 P14), B6 GFP[+]D[b]GP$_{33-41}$ TCR-tg (GFP P14), B6 CFP[+]D[b]GP$_{33-41}$ TCR-tg (CFP P14), B6 H-2D[b−/−], and B6 CD11c-YFP mice were bred and maintained in closed facilities at the National Institutes of Health, The Scripps Research Institute, and New York University. B6, Ly5.1, and OT-I mice were originally purchased from The Jackson Laboratory. CD11c-YFP mice (gift from M. Nussenzweig, Rockefeller University, New York, NY; Lindquist et al., 2004) were backcrossed for three additional generations to obtain mice on a pure C57BL/6J background. After backcrossing, the mice were confirmed to be C57BL/6J by SNP analysis (Taconic). All mice were handled in accordance with the guidelines set forth by the National Institutes of Health Animal Care and Use Committee.

Viruses. Animals were infected i.c. with 10³ PFU LCMV Arm clone 53b or i.v. with 10⁶ PFU VSV-OVA (gift from L. Lefrancois, University of Connecticut Health Center, Farmington, CT; Vezys et al., 2000). A three-segment

recombinant of LCMV expressing TFP was generated as described previously (r3LCMV-TFP; Emonet et al., 2009). In brief, we generated an LCMV recombinant containing one L and two S segments. The entire 708-bp coding region for TFP (Allele Biotech) was PCR amplified using primers (5′-GAGCAACAAGGTGTCTTCTAGTATGGTGAGCAAGGGCGA-GGAG-3′ and 5′-AGGGTCTTGTCTTCTCACAACATTTGGGCC-TCTAAAAATTAGGTCATGTGGCAGAATGTTGGCTAGCAGGCC-TTCACTTGTACAGCTCGTCCATG-3′) containing BbsI sites and subsequently cloned into a vector containing the LCMV S genomic segment backbone (pol-I GPC/BbsI; Emonet et al., 2009). r3LCMV-TFP was then rescued by transfecting 70% confluent BHK-21 cells with five plasmids (0.8 µg pC-NP, 1.0 µg pC-L, 1.4 µg pol-I L, 0.8 µg pol-I BsmBI/NP, and 0.8 µg pol-I GPC/TFP) using Lipofectamine-2000 (Invitrogen). At 72 h after transfection, the cell culture supernatant was passed to a fresh cell monolayer to isolate LCMV-TFP by plaque purification. The virus isolates were further passaged five times in BHK-21 cells, after which viral stocks were generated for subsequent animal experiments. Because three segment LCMV recombinants are attenuated compared with WT virus (Emonet et al., 2009), we infected mice i.c. with 10^6 PFU r3LCMV-TFP to induce meningitis with normal disease kinetics.

Mononuclear cell isolations. To obtain cell suspensions for flow cytometric analysis and sorting, brains were harvested from mice after an intracardiac perfusion with 20 ml of 0.9% saline solution to remove the contaminating blood lymphocytes. The CNS was incubated with 1 ml collagenase D (1 mg/ml; Roche) at 37°C for 30 min. Single-cell suspensions were prepared by mechanical disruption through a 100-µm filter. Brain-infiltrating leukocytes were isolated and counted as described previously (Lauterbach et al., 2006).

Flow cytometry. Leukocytes harvested from the brain, blood, cervical LNs, and spleen were blocked with 3.3 µg/ml anti–mouse CD16/CD32 (Fc Block; BD) in PBS containing 1% FBS and 0.1% sodium azide for 10 min on ice. Cells were surfaced stained with a combination of the following conjugated antibodies: CD45.2 FITC (104), CD11c PE (HL3), Thy1.1 PE (Ox-7), Thy1.2 PE (53–2.1; BD), gp38 PE (8.1.1), CD80 PerCP Cy5.5 (16-10A1), IA/IE PerCP Cy5.5 (M5/114.15.2), CD86 APC (GL-1), H2 K^bD^b FITC (28–8-6), CD11c Pacific Blue (N418), CD45.2 Alexa Fluor 700 (104; BioLegend), CD8 Pacific Blue (Invitrogen), CD44 FITC (IM7), CD62L PECy7 (MEL-14), and anti-CD11b PE/Cy7 (M1/70; eBioscience) for 20 min on ice. Cell cycle staining was conducted according to manufacturer's instructions using the BrdU APC cell cycle analysis kit (BD). In some cases, PE-conjugated antibodies against granzyme B (GB11) or an isotype control (Invitrogen) were added at the same time as the BrdU APC staining to examine granzyme expression during cell cycle. Cells were acquired using a digital flow cytometer (Digital LSR II; BD) and flow cytometric data were analyzed with FlowJo software (Tree Star, Inc).

CD8+ T cell isolations. CD8+ T cells were purified from Thy1.1+ P14, GFP+ P14, CFP+ P14, or Ly5.2+ OT-I mouse splenocytes by negative selection (STEMCELL Technologies). The purity after enrichment was determined to be >98%. For imaging and flow cytometric studies, 10^4 purified naive P14 or OT-I T cells were injected i.v. into naive mice. Mice were subsequently challenged with LCMV Arm or VSV-OVA.

In vivo BrdU studies. Animals were seeded with 10^4 Thy1.1+ P14 cells before i.c. infection with 10^3 PFU LCMV Arm or 10^4 Ly5.2+ OT-I cells before i.v. infection with 10^6 PFU VSV-OVA. On day 6 after LCMV infection, animals were injected i.p. with 2 mg BrdU (Sigma–Aldrich) for 15 min. VSA-OVA–infected mice were injected with BrdU at day 5 after infection. Blood was collected from animals before perfusion with 20 ml saline. The brain, spleen, liver, and cervical LNs were harvested and single cell suspensions were generated from all of these organs. Cells were surfaced stained with antibodies to detect Thy1.1+ P14 or Ly5.2+ OT-I CD8 T cells and then further fixed, permeabilized, and stained for BrdU and 7AAD according to the BrdU APC flow cytometry kit manufacturer's instructions (BD). For BrdU studies in

which peptide was injected into the subarachnoid space, Thy1.1+ P14 seeded animals were infected with 10^3 PFU LCMV Arm. On day 6 after infection, animals were anaesthetized and 10 mg/ml BrdU was mixed with 0.17 mg/ml GP_{33-41} or $OVA_{257-264}$ peptide was administered into the subarachnoid space of the brain through a small open skull preparation and incubated for 30 min. 10 mg/ml BrdU alone was then incubated for another hour before saline perfusion and isolation of Thy1.1 P14 cells from the brain for analysis of BrdU incorporation by flow cytometry.

In vitro BrdU studies. Splenocytes of 10^4 Thy1.1+ P14 seeded animals were harvested on day 6 after i.c. infection with 10^3 PFU LCMV Arm. Cells were stained with anti-Thy1.1 PE (BD), CD8 APC-Cy7 (BioLegend), and 7AAD (BD) in 2% FBS/PBS for 20 min on ice. Virus-specific T cells were sorted for Thy1.1+ CD8+ 7AAD− cells to a purity of >95%. To generate CNS APCs, the microglia and mononuclear infiltrates in brains from PBS perfused day-6 i.c LCMV-infected C57BL/6 animals were isolated and pulsed with 1 µg/ml GP_{33-41} peptide in RPMI complete (10% FBS, 10 U/ml penicillin, 10 µg/ml streptomycin, 2 mM glutamine, and 50 uM β–mercaptoethanol; Invitrogen) for 1 h at 37°C. Cells were washed and stained with anti-Thy1.2 APC (BioLegend), CD11b PE/Cy7 (eBioscience), CD11c APC/Cy7 (BioLegend), and CD45.2 FITC and 7AAD (BD) in 2% FBS/PBS for 20 min on ice. Thy1.2− 7AAD− cells were sorted into three groups: microglia (CD45^{lo} CD11b+), macrophage/monocytes (CD45^{hi} CD11b+ CD11c−), and DCs (CD45^{hi} CD11b+ CD11c+). All cells were sorted on a FACSAria Digital Cell Sorter (BD). Splenic DCs obtained from day-6 i.c. LCMV-infected C57BL/6 animals were stained and sorted by the same criteria as CNS DCs. Thy1.1+ P14 cells were plated with sorted CNS APCs at a ratio of 2:1, centrifuged for 5 min to increase cell–cell interactions, and incubated for 90 min at 37°C at 5% humidity. For in vitro stimulation, splenic DCs were plated at the same T cell/DC ratio and 1 µg/ml peptide, either $OVA_{257-264}$ (SIINFEKL) or GP_{33-41} (KAVYNFATC), was added to the wells for the duration of the 90-min incubation. During the last 30 min of culture, cells were pulsed with 10 µM BrdU. Cultures were harvested, Fc blocked for 15 min on ice, surface stained with anti-Thy1.1 PE (BD) and CD8 Pacific blue (Caltag) for 20 min on ice, and analyzed for cell cycle according to the BrdU APC flow kit manufacturer's instructions (BD). Normalized cell cycle percentages in Fig. 5 (D and E) were calculated by dividing individual percentages by the highest value in the group for that experiment.

Thy1.1+ P14 transfers into H-2D$^{b-/-}$ mice. CD8+ T cells were purified from mice seeded with 10^4 Thy1.1+ P14 cells on day 6 after i.c. infection using CD8+ beads (Miltenyi Biotec). 20–30 × 10^6 CD8+ T cells (∼2.5–3 × 10^6 Thy1.1+ P14 CTL) were injected retroorbitally into C57BL/6 or H-2D$^{b-/-}$ mice at day 6–6.5 after infection with 10^3 PFU LCMV Arm i.c. 90 min after T cell transfer, animals were injected with 2 mg BrdU i.p. for 15 min, PBS perfused, and the brains were harvested. Cells were stained as indicated in the in vivo BrdU portion of the methods section.

Immunohistochemistry. To examine virus-specific CTL cell division, brains from 10^4 P14 GFP+ seeded mice were perfused with 4% PFA (Sigma–Aldrich) on day 6 after infection with 10^3 PFU LCMV Arm i.c. Brains were frozen in O.C.T. (VWR) after an overnight incubation in 4% PFA followed by an overnight incubation in 30% sucrose (Thermo Fisher Scientific). 6-µm frozen sections were cut, fixed with 4% paraformaldehyde for 15 min, blocked with an avidin/biotin-blocking kit (Vector Laboratories), and stained at 4°C overnight with primary rabbit antibodies against Ki-67 (1:50; Leica). The primary antibody was detected with donkey anti–rabbit rhodamine red-X for 1 h at room temperature (1:200; Jackson ImmunoResearch Laboratories, Inc.). Sections were further stained with 1 µg/ml DAPI (Sigma–Aldrich) for 3 min at room temperature to visualize cell nuclei. All working stocks of primary and secondary reagents were diluted in PBS containing 2% FBS.

Confocal microscopy. 2D colocalization images to analyze Ki-67 staining in GFP+ P14 CTL were captured from 6-µm frozen brain sections using a MRC2100 confocal microscope (Bio-Rad Laboratories) fitted with 40, 63, and 100× oil objectives and seven laser lines that excite at 405, 457, 477, 488, 514, 543, and 637 nm (Carl Zeiss).

Intravital two-photon microscopy. Mice were anaesthetized and maintained at a core temperature of 37°C. Thinned skull and open skull preparations were performed to visualize GFP⁺ P14 cells, rhodamine-2AM, and quantum dots as described previously (Kim et al., 2009; Yang et al., 2010). Imaging data shown in Figs. 4 and 8, part of Fig. S2, and Videos 1 and 2 were collected using an SP5 two-photon imaging system (Leica) equipped with an 8,000-Hz resonant scanner, a 20×/1.0 NA dipping objective, and a Mai Tai HP DeepSee Laser (Spectra-Physics) tuned to 920 nm. Fluorescence emission was separated by high-efficiency custom dichroic mirrors (Semrock) and collected with an NDD4 external detector (Leica). Stacks of images were acquired using a step size of 2.5 µm to a depth of 50 µm. Time-lapse videos were acquired with 30-s intervals between 3D stacks. Imaging data shown in Fig. 6, Fig. S2, and Videos 1 and 3 were obtained using a Radiance multiphoton microscope (Carl Zeiss) powered by a Tsunami pulsed laser (Spectra-Physics) and an LSM 710 (Carl Zeiss) powered by a Mai Tai DeepSee tuned to 920 nm as described previously (Kim et al., 2009). To visualize meningeal vasculature, mice were injected i.v. 10 min before imaging with 50 µl of Qtracker nontargeted quantum dots (655 nm; 0.2 µM; Invitrogen). For rhodamine-2AM studies, 20 µM rhod2-AM (Invitrogen) in 200 µl of artificial cerebral spinal fluid (119 mM NaCl, 26.2 mM NaHCO₃, 2.5 mm KCl, 1 mM NaH₂PO₄, 1.3 mM MgCl₂, 1.2 mM CaCl₂, and 0.4% glucose, pH 7.4) was administered through a partially open skull adjacent to the thinned skull viewing area. The compound was incubated for 30 min to permit adequate local tissue diffusion. CTL dynamics were imaged through the adjacent thinned skull. For CNS peptide studies, 1 mg/ml GP₃₃₋₄₁ or OVA₂₅₇₋₂₆₄ peptide was administered through a craniotomy adjacent to the thinned skull window. Imaging through the thinned skull region was conducted within the first hour after peptide delivery. All quantitative analyses and tracking of cell movements shown in Figs. 4 and 8 were performed using Imaris 7.0 software (Bitplane). Mean track velocities (in micrometers per minute) and motility coefficients (in micrometers squared per minute) were calculated for individual tracks spanning 11 time points (or 5 min). The motility coefficient was defined as the slope of the fitted line of displacement squared versus time. Instantaneous track velocities (in micrometers per minute) were also calculated and plotted versus time (Zinselmeyer et al., 2009). All track calculations were performed using T cell Analyzer version 1.7.0 software (written by J. Dempster, University of Strathclyde, Glasgow, Scotland). Dividing CTLs were defined as those that underwent mitosis in a 4D video. All analyses shown in Fig. 6 and Fig. S2 B were performed using Volocity software (PerkinElmer). The mean velocities (in micrometers per minute) of CTLs adjacent to YFP⁺ DCs were quantified manually from 30-min time lapses with 20 intervals. Contact duration (in minutes) is the total time that a CTL remained in contact with a DC during the 30-min time lapse. "Mobile" CTLs were defined as those having a mean velocity of >2 µm/min during DC contact, whereas "stable" CTLs had velocities of ≤2 µm/min during DC contact.

CTLA-4-Fc treatment. Mice seeded with 10⁴ Thy1.1 P14 cells were infected with 10³ PFU LCMV Arm i.c. On days 4 and 5 after infection, mice were injected i.p. with 200 µg CTLA-4-Fc (Sigma-Aldrich) or an equal volume of PBS (Invitrogen). In vivo BrdU studies were conducted on day 6 after infection.

Statistical analysis. Statistical significance ($P < 0.05$) was determined using a Student's t test, a Mann-Whitney rank sum test for populations with non-Gaussian distributions, or a one-way ANOVA for experiments containing more than two groups.

Online supplemental material. Fig. S1 shows that virus-specific CTLs circulate in cell cycle after VSV infection. Fig. S2 shows representative time lapses of CTL undergoing mitosis after arrest in the meninges. Fig. S3 shows that LCMV is detected in both resident and CNS-infiltrating APCs at day 6 after infection. Video 1 shows examples of CTL division in the virally infected meninges. Video 2 shows anatomy and dynamics of CTL division in the virally infected meninges. Video 3 shows that CTLs divide with and without contacting meningeal DCs. Online supplemental material is available at http://www.jem.org/cgi/content/full/jem.20101295/DC1.

REFERENCES

Agarwal, P., A. Raghavan, S.L. Nandiwada, J.M. Curtsinger, P.R. Bohjanen, D.L. Mueller, and M.F. Mescher. 2009. Gene regulation and chromatin remodeling by IL-12 and type I IFN in programming for CD8 T cell effector function and memory. *J. Immunol.* 183:1695–1704. doi:10.4049/jimmunol.0900592

Bajénoff, M., O. Wurtz, and S. Guerder. 2002. Repeated antigen exposure is necessary for the differentiation, but not the initial proliferation, of naive CD4(+) T cells. *J. Immunol.* 168:1723–1729.

Bartholomäus, I., N. Kawakami, F. Odoardi, C. Schläger, D. Miljkovic, J.W. Ellwart, W.E. Klinkert, C. Flügel-Koch, T.B. Issekutz, H. Wekerle, and A. Flügel. 2009. Effector T cell interactions with meningeal vascular structures in nascent autoimmune CNS lesions. *Nature.* 462:94–98. doi:10.1038/nature08478

Celli, S., Z. Garcia, and P. Bousso. 2005. CD4 T cells integrate signals delivered during successive DC encounters in vivo. *J. Exp. Med.* 202:1271–1278. doi:10.1084/jem.20051018

Croft, M., L.M. Bradley, and S.L. Swain. 1994. Naive versus memory CD4 T cell response to antigen. Memory cells are less dependent on accessory cell costimulation and can respond to many antigen-presenting cell types including resting B cells. *J. Immunol.* 152:2675–2685.

Dean, P.N., F. Dolbeare, H. Gratzner, G.C. Rice, and J.W. Gray. 1984. Cell-cycle analysis using a monoclonal antibody to BrdUrd. *Cell Tissue Kinet.* 17:427–436.

Emonet, S.F., L. Garidou, D.B. McGavern, and J.C. de la Torre. 2009. Generation of recombinant lymphocytic choriomeningitis viruses with trisegmented genomes stably expressing two additional genes of interest. *Proc. Natl. Acad. Sci. USA.* 106:3473–3478. doi:10.1073/pnas.0900088106

Engelhardt, B., and R.M. Ransohoff. 2005. The ins and outs of T-lymphocyte trafficking to the CNS: anatomical sites and molecular mechanisms. *Trends Immunol.* 26:485–495. doi:10.1016/j.it.2005.07.004

Faroudi, M., R. Zaru, P. Paulet, S. Müller, and S. Valitutti. 2003. Cutting edge: T lymphocyte activation by repeated immunological synapse formation and intermittent signaling. *J. Immunol.* 171:1128–1132.

Flügel, A., T. Berkowicz, T. Ritter, M. Labeur, D.E. Jenne, Z. Li, J.W. Ellwart, M. Willem, H. Lassmann, and H. Wekerle. 2001. Migratory activity and functional changes of green fluorescent effector cells before and during experimental autoimmune encephalomyelitis. *Immunity.* 14:547–560. doi:10.1016/S1074-7613(01)00143-1

Friedman, R.S., P. Beemiller, C.M. Sorensen, J. Jacobelli, and M.F. Krummel. 2010. Real-time analysis of T cell receptors in naive cells in vitro and in vivo reveals flexibility in synapse and signaling dynamics. *J. Exp. Med.* 207:2733–2749. doi:10.1084/jem.20091201

Garidou, L., S. Heydari, P. Truong, D.G. Brooks, and D.B. McGavern. 2009. Therapeutic memory T cells require costimulation for effective clearance of a persistent viral infection. *J. Virol.* 83:8905–8915. doi:10.1128/JVI.00027-09

Gett, A.V., F. Sallusto, A. Lanzavecchia, and J. Geginat. 2003. T cell fitness determined by signal strength. *Nat. Immunol.* 4:355–360. doi:10.1038/ni908

Gunzer, M., A. Schäfer, S. Borgmann, S. Grabbe, K.S. Zänker, E.B. Bröcker, E. Kämpgen, and P. Friedl. 2000. Antigen presentation in extracellular matrix: interactions of T cells with dendritic cells are dynamic, short lived, and sequential. *Immunity.* 13:323–332. doi:10.1016/S1074-7613(00)00032-7

Iezzi, G., K. Karjalainen, and A. Lanzavecchia. 1998. The duration of antigenic stimulation determines the fate of naive and effector T cells. *Immunity.* 8:89–95. doi:10.1016/S1074-7613(00)80461-6

Kang, S.S., and D.B. McGavern. 2008. Lymphocytic choriomeningitis infection of the central nervous system. *Front. Biosci.* 13:4529–4543. doi:10.2741/3021

Kawakami, N., S. Lassmann, Z. Li, F. Odoardi, T. Ritter, T. Ziemssen, W.E. Klinkert, J.W. Ellwart, M. Bradl, K. Krivacic, et al. 2004. The activation status of neuroantigen-specific T cells in the target organ determines the clinical outcome of autoimmune encephalomyelitis. *J. Exp. Med.* 199:185–197. doi:10.1084/jem.20031064

Kawakami, N., U.V. Nägerl, F. Odoardi, T. Bonhoeffer, H. Wekerle, and A. Flügel. 2005. Live imaging of effector cell trafficking and autoantigen recognition within the unfolding autoimmune encephalomyelitis lesion. *J. Exp. Med.* 201:1805–1814. doi:10.1084/jem.20050011

Kim, J.V., S.S. Kang, M.L. Dustin, and D.B. McGavern. 2009. Myelomonocytic cell recruitment causes fatal CNS vascular injury during acute viral meningitis. *Nature.* 457:191–195. doi:10.1038/nature07591

Lauterbach, H., E.I. Zuniga, P. Truong, M.B. Oldstone, and D.B. McGavern. 2006. Adoptive immunotherapy induces CNS dendritic cell recruitment and antigen presentation during clearance of a persistent viral infection. *J. Exp. Med.* 203:1963–1975. doi:10.1084/jem.20060039

Li, Q., P.J. Skinner, S.J. Ha, L. Duan, T.L. Mattila, A. Hage, C. White, D.L. Barber, L. O'Mara, P.J. Southern, et al. 2009. Visualizing antigen-specific and infected cells in situ predicts outcomes in early viral infection. *Science.* 323:1726–1729. doi:10.1126/science.1168676

Lindquist, R.L., G. Shakhar, D. Dudziak, H. Wardemann, T. Eisenreich, M.L. Dustin, and M.C. Nussenzweig. 2004. Visualizing dendritic cell networks in vivo. *Nat. Immunol.* 5:1243–1250. doi:10.1038/ni1139

Ling, C., M. Sandor, M. Suresh, and Z. Fabry. 2006. Traumatic injury and the presence of antigen differentially contribute to T-cell recruitment in the CNS. *J. Neurosci.* 26:731–741. doi:10.1523/JNEUROSCI.3502-05.2006

Ling, C., Y.I. Verbny, M.I. Banks, M. Sandor, and Z. Fabry. 2008. In situ activation of antigen-specific CD8+ T cells in the presence of antigen in organotypic brain slices. *J. Immunol.* 180:8393–8399.

Linsley, P.S., P.M. Wallace, J. Johnson, M.G. Gibson, J.L. Greene, J.A. Ledbetter, C. Singh, and M.A. Tepper. 1992. Immunosuppression in vivo by a soluble form of the CTLA-4 T cell activation molecule. *Science.* 257:792–795. doi:10.1126/science.1496399

Masopust, D., K. Murali-Krishna, and R. Ahmed. 2007. Quantitating the magnitude of the lymphocytic choriomeningitis virus-specific CD8 T-cell response: it is even bigger than we thought. *J. Virol.* 81:2002–2011. doi:10.1128/JVI.01459-06

McGavern, D.B., U. Christen, and M.B. Oldstone. 2002. Molecular anatomy of antigen-specific CD8(+) T cell engagement and synapse formation in vivo. *Nat. Immunol.* 3:918–925. doi:10.1038/ni843

Mescher, M.F., J.M. Curtsinger, P. Agarwal, K.A. Casey, M. Gerner, C.D. Hammerbeck, F. Popescu, and Z. Xiao. 2006. Signals required for programming effector and memory development by CD8 T cells. *Immunol. Rev.* 211:81–92. doi:10.1111/j.0105-2896.2006.00382.x

Miller, M.J., O. Safrina, I. Parker, and M.D. Cahalan. 2004. Imaging the single cell dynamics of CD4+ T cell activation by dendritic cells in lymph nodes. *J. Exp. Med.* 200:847–856. doi:10.1084/jem.20041236

Murali-Krishna, K., J.D. Altman, M. Suresh, D.J. Sourdive, A.J. Zajac, J.D. Miller, J. Slansky, and R. Ahmed. 1998. Counting antigen-specific CD8 T cells: a reevaluation of bystander activation during viral infection. *Immunity.* 8:177–187. doi:10.1016/S1074-7613(00)80470-7

Pircher, H., K. Bürki, R. Lang, H. Hengartner, and R.M. Zinkernagel. 1989. Tolerance induction in double specific T-cell receptor transgenic mice varies with antigen. *Nature.* 342:559–561. doi:10.1038/342559a0

Salomon, B., and J.A. Bluestone. 2001. Complexities of CD28/B7: CTLA-4 costimulatory pathways in autoimmunity and transplantation. *Annu. Rev. Immunol.* 19:225–252. doi:10.1146/annurev.immunol.19.1.225

van Heijst, J.W., C. Gerlach, E. Swart, D. Sie, C. Nunes-Alves, R.M. Kerkhoven, R. Arens, M. Correia-Neves, K. Schepers, and T.N. Schumacher. 2009. Recruitment of antigen-specific CD8+ T cells in response to infection is markedly efficient. *Science.* 325:1265–1269. doi:10.1126/science.1175455

van Stipdonk, M.J., E.E. Lemmens, and S.P. Schoenberger. 2001. Naïve CTLs require a single brief period of antigenic stimulation for clonal expansion and differentiation. *Nat. Immunol.* 2:423–429.

van Stipdonk, M.J., G. Hardenberg, M.S. Bijker, E.E. Lemmens, N.M. Droin, D.R. Green, and S.P. Schoenberger. 2003. Dynamic programming of CD8+ T lymphocyte responses. *Nat. Immunol.* 4:361–365. doi:10.1038/ni912

Veiga-Fernandes, H., U. Walter, C. Bourgeois, A. McLean, and B. Rocha. 2000. Response of naïve and memory CD8+ T cells to antigen stimulation in vivo. *Nat. Immunol.* 1:47–53. doi:10.1038/76907

Vezys, V., S. Olson, and L. Lefrançois. 2000. Expression of intestine-specific antigen reveals novel pathways of CD8 T cell tolerance induction. *Immunity.* 12:505–514. doi:10.1016/S1074-7613(00)80202-2

Wakim, L.M., J. Waithman, N. van Rooijen, W.R. Heath, and F.R. Carbone. 2008. Dendritic cell-induced memory T cell activation in nonlymphoid tissues. *Science.* 319:198–202. doi:10.1126/science.1151869

Wilson, E.H., T.H. Harris, P. Mrass, B. John, E.D. Tait, G.F. Wu, M. Pepper, E.J. Wherry, F. Dzierzinski, D. Roos, et al. 2009. Behavior of parasite-specific effector CD8+ T cells in the brain and visualization of a kinesis-associated system of reticular fibers. *Immunity.* 30:300–311. doi:10.1016/j.immuni.2008.12.013

Xu, H.T., F. Pan, G. Yang, and W.B. Gan. 2007. Choice of cranial window type for in vivo imaging affects dendritic spine turnover in the cortex. *Nat. Neurosci.* 10:549–551. doi:10.1038/nn1883

Yang, G., F. Pan, C.N. Parkhurst, J. Grutzendler, and W.B. Gan. 2010. Thinned-skull cranial window technique for long-term imaging of the cortex in live mice. *Nat. Protoc.* 5:201–208. doi:10.1038/nprot.2009.222

Zinselmeyer, B.H., J. Dempster, D.L. Wokosin, J.J. Cannon, R. Pless, I. Parker, and M.J. Miller. 2009. Chapter 16. Two-photon microscopy and multi-dimensional analysis of cell dynamics. *Methods Enzymol.* 461:349–378. doi:10.1016/S0076-6879(09)05416-0